Eur. Phys. J. A **13**, 435–448 (2002)
DOI 10.1140/epja/iepja1221

THE EUROPEAN PHYSICAL JOURNAL A

Lifetimes in the ground-state band and the structure of ^{118}Te

A.A. Pasternak[1,2], J. Srebrny[2], A.D. Efimov[1], V.M. Mikhajlov[3], E.O. Podsvirova[1], Ch. Droste[2], T. Morek[2], S. Juutinen[4], G.B. Hagemann[5], M. Piiparinen[4], S. Törmänen[5], and A. Virtanen[4]

[1] Cyclotron Laboratory, A.F. Ioffe Physical Technical Institute, 194021, St. Petersburg, Russia
[2] Nuclear Physics Division, IEP, Warsaw University, Hoża 69, 00-681 Warsaw, Poland
[3] Physical Institute of St. Petersburg State University, 198904, St. Petersburg, Russia
[4] Department of Physics, University of Jyväskylä, P.O Box 35, FIN-40351, Jyväskylä, Finland
[5] The Niels Bohr Institute, Blegdamsvej 17, DK-2100, Copenhagen, Denmark

Received: 7 June 2001 / Revised version: 28 January 2002
Communicated by D. Schwalm

Abstract. Lifetimes of excited states in ^{118}Te have been measured using the Doppler Shift Attenuation (DSA) and Recoil Distance (RD) methods in the ^{109}Ag(^{13}C, p3n) reaction at a beam energy of 54 MeV. Lifetime values of the ground-state band levels with spins $I^\pi = 2^+$–16^+ have been obtained. The excitation energies and $B(E2)$ values are interpreted in the framework of a version of IBFM (IBM + 2qp) with the maximum boson number exceeding its standard value. A satisfactory agreement with experimental level scheme and $B(E2)$ values for the ground-state band is achieved.

PACS. 21.10.Tg Lifetimes – 21.60.Fw Models based on group theory – 23.20.Lv Gamma transitions and level energies – 27.60.+j $90 \leq A \leq 149$

1 Introduction

The present work is a continuation of the systematic investigation of the electromagnetic properties of the nuclei with $N = 66$. Previously, the lifetime values in ^{119}I were determined for 10 bands [1–3]. On the basis of 65 measured lifetimes, the complex level structure was interpreted and shape coexistence has been deduced. Compared to ^{119}I the information on electromagnetic transition probabilities for the even-even isotones ^{120}Xe and ^{118}Te was rather poor. Only very recently 22 lifetimes of excited states up to $I^\pi = 22^+$ in ^{120}Xe have been measured by the DSA method in the ^{111}Cd(^{13}C, 3n) reaction [4]. For ^{118}Te some lifetimes have been determined using the DSA method in the ^{116}Sn(α, 2n) reaction [5], but only for the 8^+ and 10^+ states of the ground-state band. Lifetimes of the 2^+, 4^+, 6^+ states and of the states with $I^\pi > 10^+$ were unknown.

The level scheme of ^{118}Te has been previously investigated using reactions induced by α-particles [6,7], and heavy ions [8,9]. High-spin states up to $I = 32^+$ have been found recently in the (^{18}O, 4n) and (^{22}Ne, 4n) reactions [10]. The experiment shows, that the ground-state band in ^{118}Te is yrast only for $I \leq 10^+$. The IBM-2 and One-Broken Pair model calculations [7] allowed to identify the higher members of the ground-state band among the levels observed in experiment. Similar results were obtained in [5] where properties of ^{118}Te were interpreted in the frame of the quasiparticle-boson extension of IBM-1. It is worth to add, that recently this approach was significantly improved and applied to other nuclei [11], in particular to the calculations of electromagnetic transition probabilities in ^{120}Xe [4].

Experimental techniques, data analysis and results of lifetimes measurement for levels belonging to the ground-state band are given in sects. 2 and 3. Some new methods of the data evaluation in the Doppler Shift Attenuation Method (DSAM) and the Recoil Distance Method (RDM) are presented also in sect. 2. Theoretical interpretation and development of the IBM-1 + 2qp model are given in sect. 4.

2 Experimental techniques and data analysis

The experiment was performed at the Tandem Accelerator Laboratory of the Niels Bohr Institute using the ^{109}Ag (^{13}C, p3n) ^{118}Te reaction at an energy of 54 MeV. The γ-γ coincidences were collected by the NORDBALL array with 20 Compton-suppressed HPGe-detectors placed at four rings at the angles of 37°, 79°, 101° and 143°. Since details of the experimental conditions and procedure of data evaluation are given in refs. [1,2,12], only a brief description is presented here. Two kinds of measurements have been performed: 1) DSA measurement with a thick target of 5.7 mg/cm^2; 2) recoil distance measurement with a plunger device installed inside the NORD-

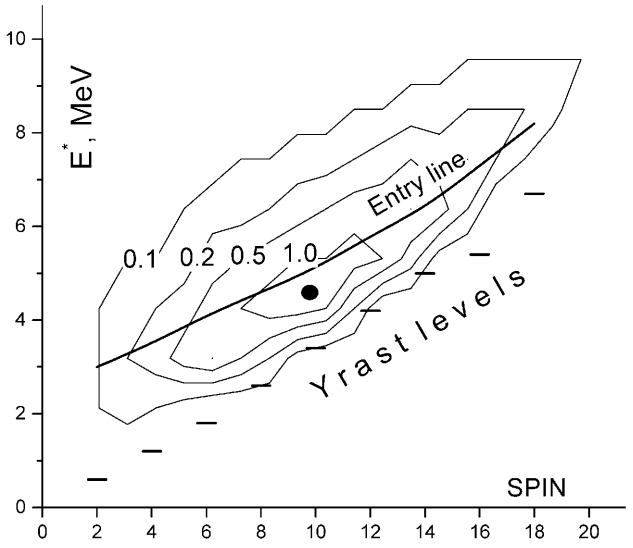

Fig. 1. Entry state population for the reaction ^{109}Ag(^{13}C, p3n) at $E = 54$ MeV. The cross-section is given in mb/(MeV$\hbar$). The entry line, being the center of gravity of the entry state population for each spin value is also shown.

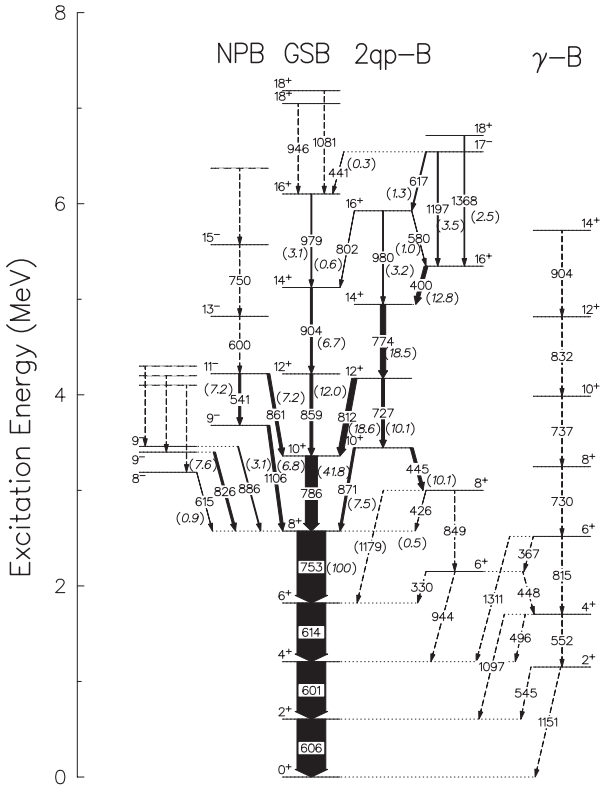

Fig. 2. Partial level scheme of ^{118}Te [9,10]. Dotted lines: levels and transitions having no influence on lifetime evaluation. Numbers in italic: relative intensities of transitions. Intensities are given with an accuracy of about 5–10%. The abbreviation NPB is the negative-parity band; GSB is the ground-state band; 2qp-B is the two-quasiparticle band; γ-B is the quasi-γ band.

BALL array using a thin target of 0.82 mg/cm^2. In both cases the spectra gated below and above the transition of interest and the sums of such gated spectra were used for the analysis. The experimental γ line shapes were analysed using an updated version of the computer codes COMPA, GAMMA and SHAPE [12] for both DSA and RDM data. Using this software, it is possible to fit groups of overlapping Doppler-broadened peaks treating level lifetimes as line shape parameters. In RDM lifetime is obtained by line shape analysis without separation of the γ line for shifted and unshifted components (RDDSA method [1,2,13,14]). To evaluate the stopping power of the recoils, the Lindhard correction factors for the electronic (f_e) and nuclear (f_n) components have been measured by line shape analysis using the "semi-thick target" method [1,2]. Values of $f_e = 1.27 \pm 0.07$ and $f_n = 0.77 \pm 0.07$ obtained for the ^{119}I recoils travelling in the ^{109}Ag target were adopted for the case of ^{118}Te recoils.

For a rough estimation of the effective side feeding time (τ_{sf}) we took into account that in our experimental conditions the residual ^{118}Te nuclei were produced in states of low excitation energy and angular momentum via the p3n channel. Excitation energy and spin dependence of the entry state population probability (cross-section) calculated with the Monte Carlo method (program COMPA) is shown in fig. 1. The maximum of the population probability, marked as a black circle in fig. 1 lies at an energy of 4.5 MeV and spin 10$\hbar$. For comparison in ^{119}I, populated via the 3n-evaporation channel from the same compound nucleus, the corresponding maximum lies at 13 MeV and 18$\hbar$ [1,2]. For the similar ^{111}Cd(^{12}C, 3n)^{120}Xe reaction at $E_C = 56$ MeV it lies at 7 MeV and 12$\hbar$ [4]. Shorter τ_{sf} values may be expected in ^{118}Te. In ^{119}I τ_{sf} values have been experimentally evaluated for high-spin states of $I \approx 16$–18 in refs. [1,2] as ≈ 0.10 ps and in ^{120}Xe [4] as ≈ 0.04 ps. Using an empirical formula for τ_{sf} evaluation, suggested in ref. [2], we predicted τ_{sf} to lie in the range 0.01–0.05 ps for the $I = 16$–18$\hbar$ levels of interest in ^{118}Te. Therefore, the influence of τ_{sf} on lifetime measurements is in our case negligible. This is a favorable situation for the DSA lifetime measurements of short-lived high-spin states in ^{118}Te.

Another important consequence of the low energy of the entry states is that the intensities of transitions decrease very fast with increasing spin. Of course this is disadvantagous for the lifetime evaluation of high-spin states but, on the other hand, the influence of long-lived cascade feeding from upper states is not crucial in these conditions. In fig. 2 a partial level scheme of ^{118}Te, relevant for our lifetime measurements and the theoretical discussion is shown. Relative intensities, normalized to the intensity of the $8^+ \rightarrow 6^+$ ground band transition are indicated.

In the ^{109}Ag + ^{13}C reaction ^{118}I is produced in the (^{13}C, 4n) channel. Therefore, the population of the 2^+–8^+ states in ^{118}Te via β-decay of ^{118}I is observed. For the 2^+, 4^+ and 6^+ levels the contribution of the β-decay to the total population is about 50%. These levels are also strongly populated in fusion reaction by cascade transitions from many bands. Moreover, some feeding transitions contain long-lived components. In this case, the optimal way of lifetime evaluation is to use plunger spectra

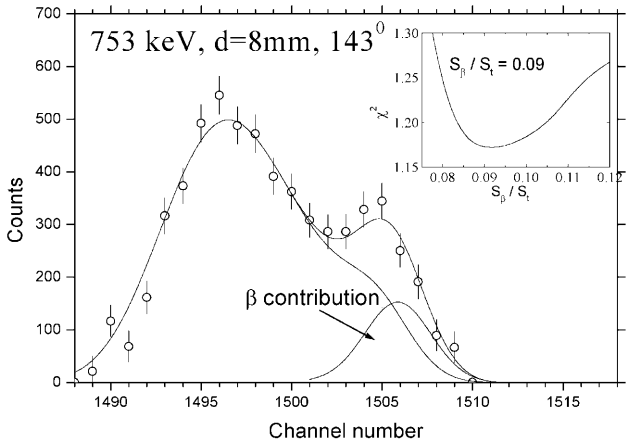

Fig. 3. Evaluation of the β-decay contribution (S_β) to the total population (S_t) of the 8^+ state using the line shape analysis of the 753 keV line at $d = 8$ mm in the plunger experiment.

taken at target-stopper distances of 15, 22, 29, 37, 42 and 52 μm obtained by gating on the flight component of the 753 keV line. Gates were set on energy range of 755–761 keV at 37° and 745–751 keV at 143°. From the line shapes analysis of the spectra resulting from these gates it was obtained that recoils decaying from 8^+ state were determined to have a velocity $v/c \geq 0.0025$ and the influence of stopped γ line components are neglegible. The information about lifetimes of the 8^+ state (753 keV line) and upper cascade feeders obtained from our DSA measurements has been taken into account in the simulation of the time evolution along the cascade.

The intensity of the 753 keV line in the spectrum gated on the 786 keV line placed above the 8^+ level is low. Therefore, the lifetime of the 8^+ state has been extracted by the DSA method from the sum of the spectra gated on the 600, 606 and 615 keV lines, located below the 753 keV transition. The evaluation of the contribution of the ^{118}I β-decay to the population of the 8^+ state is very important. For this purpose we used the line shape analysis of the 753 keV line observed in the plunger spectrum at maximal distance $d = 8$ mm where the unshifted component of this line comes from β-decay (fig. 3).

Contribution of the p3n channel to the unshifted component is negligible. To evaluate the β-decay contribution from the experimental line shape an asymmetric shape of the shifted 753 keV line component has been calculated taking into account the stopping and multiple scattering of recoils in the 0.82 mg/cm^2 thick target.

Although the shortest stopper-target distance of $d = 15$ μm is the optimal for lifetimes in the range 1–5 ps, the intensity of peaks in the gated spectra are often not sufficient for an analysis. Instead, we used the summed plunger spectra at target-stopper distances: 15, 22 and 29 μm ($d1$) as well as 37, 42 and 52 μm ($d2$). Then, the sensitivity of the lifetime determination was slightly decreased since the mean distance increased (*i.e.*, $d \approx 22$ μm instead of $d = 15$ μm). At the same time the reliability and accuracy increased due to significantly better statistics of the spectrum.

For the DSA lifetime evaluation of short-lived high-spin levels another methodical approach is used. The peak areas in the gated spectra for fixed angles (in our case 37° and 143°) are often too low to distinguish the peaks from the background. In the present work we have used in a few cases summed spectra from all 20 NORDBALL detectors. Then the resulting shapes of the Doppler broadened γ lines are symmetrical. It is useful for identification of the Doppler effect and for taking into account the influence of neighboring impurity peaks.

3 Experimental results

Results of our lifetime measurements are presented in table 1. Effective lifetimes of all levels which are not included in table 1 and marked in fig. 2 by solid lines have been deduced from the DSA thick-target experiment. They are longer than 2 ps. These levels were taken into account as cascade feeders in the DSAM lifetime evaluations for states with $I \geq 8$. For these levels there is no need to know precisely the lifetime of feeders since their effective lifetimes ($\tau \geq 2$ ps) are significantly larger than the characteristic recoil stopping time.

3.1 Levels with $I^\pi = 2^+, 4^+, 6^+$

The results of the RDDSA line shape analysis of the plunger spectra, gated on the flight component of the 753 keV transitions are presented in fig. 4. Apart from the 606, 601 and 614 keV lines, corresponding to the $2^+ \rightarrow 0^+$, $4^+ \rightarrow 2^+$, $6^+ \rightarrow 4^+$ transitions, two additional background peaks with unshifted energies of 611 and 622 keV are present in a complex group of 5 overlapping Doppler-broadened lines. These peaks, visible in the plunger spectra as fully shifted components, are also observed in the thick-target spectra.

The effective lifetime of the 6^+ state is shorter than the effective lifetimes of the 4^+ and 2^+ levels. It is measurable only at small target-stopper distances. As one can see from fig. 4 for $d = 15$ μm and for the summed spectrum $d1$, the 614 keV γ line at 15μm has a larger unshifted component than at the distance $d1$, but the intensity of the spectrum at $d1$ is 3 times higher than at 15 μm. Finally, the sensitivity for line shape evaluation at both distances are comparable.

The 4^+ state decaying via the 601 keV γ line has a much longer effective lifetime than the 6^+ level due to cascade population. The distance $d1$ with mean value $\approx$ 22 μm is nearly optimal for the lifetime determination of this level. Then shifted and unshifted components have similar intensities. Results of the fit for the 15 μm, $d1$ and $d2$ spectra have been taken into account in the lifetime evaluation.

The 2^+ state has the longest τ among the considered states. Due to cascade feeding its effective lifetime (about 18 ps) is much longer than τ itself. Therefore, the 15 μm spectrum, in which the shifted component of the 606 keV γ line appears as a small tail with low statistics, is not

Table 1. Lifetimes of excited states in ^{118}Te. Lines used for gating: g3: (606 + 601 + 614) keV; g4a: (606+614+753+786) keV; g5a: (606+601+614+753+786) keV; g9a: (944 + 849 + 445 + 727 + 774 + 812 + 1178 + 329) keV; g15a: g9a + g5a + 400a keV. Spectra summed over the distances: $d1 = 15 + 22 + 29$ μm; $d2 = 37 + 42 + 52$ μm. "a" indicates that spectra were summed over all 20 NORDBALL detectors. "fl" means gating on the flight component of the corresponding line.

J^{π}_{Band}	E_{γ} (keV)	τ (ps)	Comments
2^{+}_{GSB}	605.7	8.8 ± 1.4	RDDSA: $d1$, $d2$; g753fl; 37°, 143°
4^{+}_{GSB}	600.7	4.4 ± 0.8	RDDSA: 15 μm, $d1$, $d2$; g753fl; 37°, 143°
6^{+}_{GSB}	614.4	3.4 ± 0.5	RDDSA: 15 μm, $d1$; g753fl; 37°, 143°
8^{+}_{GSB}	753.1	$1.2^{+0.4}_{-0.3}$	DSA: g3; 37°, 143° and RDDSA: 15 μm, $d1$; g786fl; 143°
10^{+}_{GSB}	786.1	$0.87^{+0.25}_{-0.17}$	DSA: g753a
12^{+}_{GSB}	859.5	0.40 ± 0.08	DSA: g5a
14^{+}_{GSB}	903.7	$0.28^{+0.06}_{-0.04}$	DSA: g4a
16^{+}_{GSB}	979.0	$0.28^{+0.10}_{-0.08}$	DSA: g5a, g859a
$16^{+}_{\mathrm{2qp\text{-}B}}$	980.1	$0.35^{+0.15}_{-0.10}$	DSA: g9a
18^{+}_{6715}	1368.5	$0.28^{+0.14}_{-0.10}$	DSA: g15a

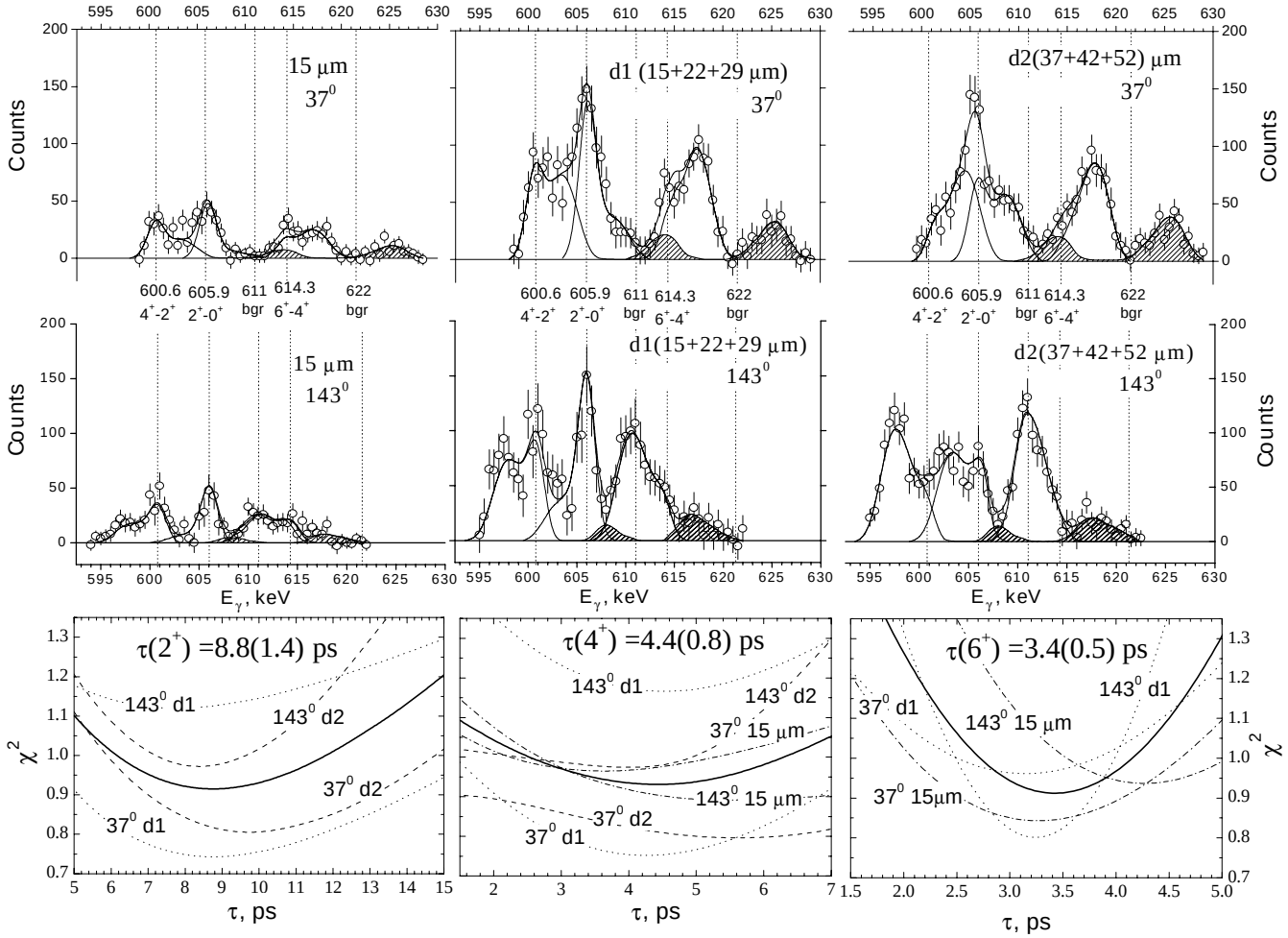

Fig. 4. Results of the RDDSA line shape analysis of plunger spectra gated on the flight component of the 753 keV $8^{+} \rightarrow 6^{+}$ line (see text for details). Fully shifted lines from contaminations are hatched, their unshifted positions are marked by "bgr". In the χ^2 plots dash-dotted, dotted and dashed lines correspond to χ^2 values for the 15 μm, $d1$ and $d2$ distances, respectively. Thick lines correspond to total χ^2 summed over data from different distances. All χ^2 values are standard χ^2 divided by the number of degrees of freedom. The energy calibration is 0.5 keV/ch.

sensitive enough for lifetime evaluation. The spectrum at the optimal distance $d2$ and also the $d1$ spectrum, were used in the lifetime evaluation.

It is worth noting that in our analysis of the plunger spectra (RDDSAM) we deal with five γ lines (including two fully shifted background peaks) instead of eight independent peaks in the traditional way of the RDM analysis. In such a complicated case with overlapping and nonsymmetrical peaks the application of the RDDSA method is the most reliable one.

3.2 Levels with I $\geq$ 8

The 8^+ *ground band level.* For a lifetime evaluation we have used the thick-target spectra at 143° and 37° and plunger spectra taken at the shortest distances. For levels with $I \geq 8$ the intensities of the γ lines taken at individual angles are too low. Therefore, thick-target spectra summed over all Ge detectors (table 1) were used. Results of the DSA line shape analysis of the 1368, 904, 859 and 786 keV lines are shown in fig. 5. The more complex cases of the DSA analysis of the 753, 979 and 980 keV γ lines are presented in figs. 6 and 7.

The 18^+ *level.* This state decays via the 1368 keV transition. For the DSA line shape analysis of the weak 1368 keV line we used the sum over 14 gated spectra (table 1). The neighboring 1363 keV line comes from contamination. It has an apparatus line shape, which was used in the fitting procedure (fig. 5a).

The 16^+ *GSB and* 16^+ $2qp$*-B levels.* According to the level scheme (fig. 2) the 979 keV line can be observed as a single line in the 859 keV (GSB) gate. Spectra gated below the 859 keV transition contain an admixture of the 980 keV transition. On the other hand the intensity of the 979 keV transition in gate 859 keV is too small for a reliable lifetime evaluation. Therefore, in addition a spectrum obtained by the sum of gates g5a (table 1) has been analyzed. The 979 and 980 keV peaks are observed in spectrum g5a as an unresolved doublet. Therefore, an independent estimate of the relative intensities of these lines and lifetime of the 16^+ 2qp-B level are needed. The lifetime of this level has been estimated from the spectrum g9a, in which the 979 keV line cannot be observed (fig. 6). For the determination of relative intensities of the 979 and 980 keV lines the sum of the 400 keV and 1197 keV lines in the spectra g5a and g9a was used for normalization, because the intensity ratio $I(980\,\mathrm{keV})/(I(400\,\mathrm{keV}) + I(1197\,\mathrm{keV}))$ should be the same in the spectra g9a and g5a. We have found that in the spectrum g5a

$$I(980\,\mathrm{keV}{+}979\,\mathrm{keV})/(I(400\,\mathrm{keV}){+}I(1197\,\mathrm{keV})) = 0.32(3)$$

and in the spectrum g9a

$$I(980\,\mathrm{keV})/(I(400\,\mathrm{keV}) + I(1197\,\mathrm{keV})) = 0.17(2);$$

therefore the ratio $I(980\,\mathrm{keV})/I(979\,\mathrm{keV}) = 1.1(2)$. To extract the lifetime of the 16^+ GSB level when both lines 979 keV and 980 keV are unresolved the information on the energy and relative intensity of these peaks and also the lifetime of the 16^+ 2qp-B level were used in the fitting procedure. The results of the analysis are shown in fig. 6. The short lifetime of the 16^+ 2qp-B level supports the 16^+ assignment which has been proposed in ref. [10]. Against the $I^\pi = 15^-$ assignment is the $B(E1)$ value which would be $\approx 10^{-3}$ W.u. for the $E1$ transition to the 14^+ state which is in contradiction with systematics of hindrance factors for $E1$ transitions.

The 14^+ *level of GSB.* For the DSA line shape analysis of the 904 keV line the spectrum g4a was used. The spectrum g5a was not used since a background peak coming from the included spectrum gated on 600 keV was found. The results are presented in fig. 5b.

The 12^+ *level of the GSB.* In the spectrum 5a, as well as in any other spectrum gated below the 10^+ level, the line 859.5 keV, corresponding to the $12^+ \rightarrow 10^+$ transition is strongly overlapping with the 861.1 keV line of the $11^- \rightarrow 10^+$ transition. Successful lifetime extraction for the 12^+ level is only possible when some parameters are fixed during the fitting procedure. The lifetime of the 11^- state is expected to be much larger than 2 ps, otherwise the $B(E2)$ value for the $11^- \rightarrow 9^-$ rotational transition would be larger than 130 W.u. (in comparison to 33 W.u. for the $2^+ \rightarrow 0^+$ transition). Therefore, the shape of the 861.1 keV line is not Doppler broadened and is close to the apparatus line shape. Small tails in this line (seen in fig. 5c) are due to some recoils which escape to vacuum from the self-supporting thick target of 5.7 mg/cm^2. The energy difference for these two peaks was fixed in the fitting procedure. From the 753 keV gate we have found the ratio $I(540.6)/I(861.1 + 859.5) = 0.37(5)$ and using the value $I(540.6)/I(861.1) = 1.0(3)$ from [10], the ratio $I(861.1)/I(859.5) = 0.59(10)$ has been obtained. The rather large uncertainty did not allow to fix this intensity ratio in the fitting procedure. Finally, two parameters: the lifetime of the 12^+ level and the intensity ratio $I(861.1)/I(859.5) = 0.61(0.08)$ have been evaluated (fig. 5c). The latter result is in good agreement with the ratio 0.59(10) discussed above.

The 10^+ *level of the GSB.* The Doppler broadening of the 786 keV γ line is small and it is difficult to distinguish it from the background. Unfortunately, the spectra gated on the 601, 606 and 614 keV lines cannot be used since they are complicated in the vicinity of the 786 keV line. The lifetime could only be evaluated in the 753 keV gate, where the 781 keV background line only slightly contaminates the 786.1 keV peak. The results are shown in fig. 5d.

The 8^+ *level of the GSB.* Difficulties with the lifetime evaluation of this level arise from a strong cascade feeding (fig. 2), and a β-decay component. In addition the lifetime of this level is too short for RDM and too long (due to cascade feeding) for DSAM. We have applied both methods (table 1 and fig. 7). In spite of a small sensitivity, the RDDSAM analysis avoids mistakes typical for DSAM in cases where it is difficult to separate Doppler tails from the background.

Our results for the 8^+ and 10^+ levels are in excellent agreement with the data of ref. [5] where lifetimes equal

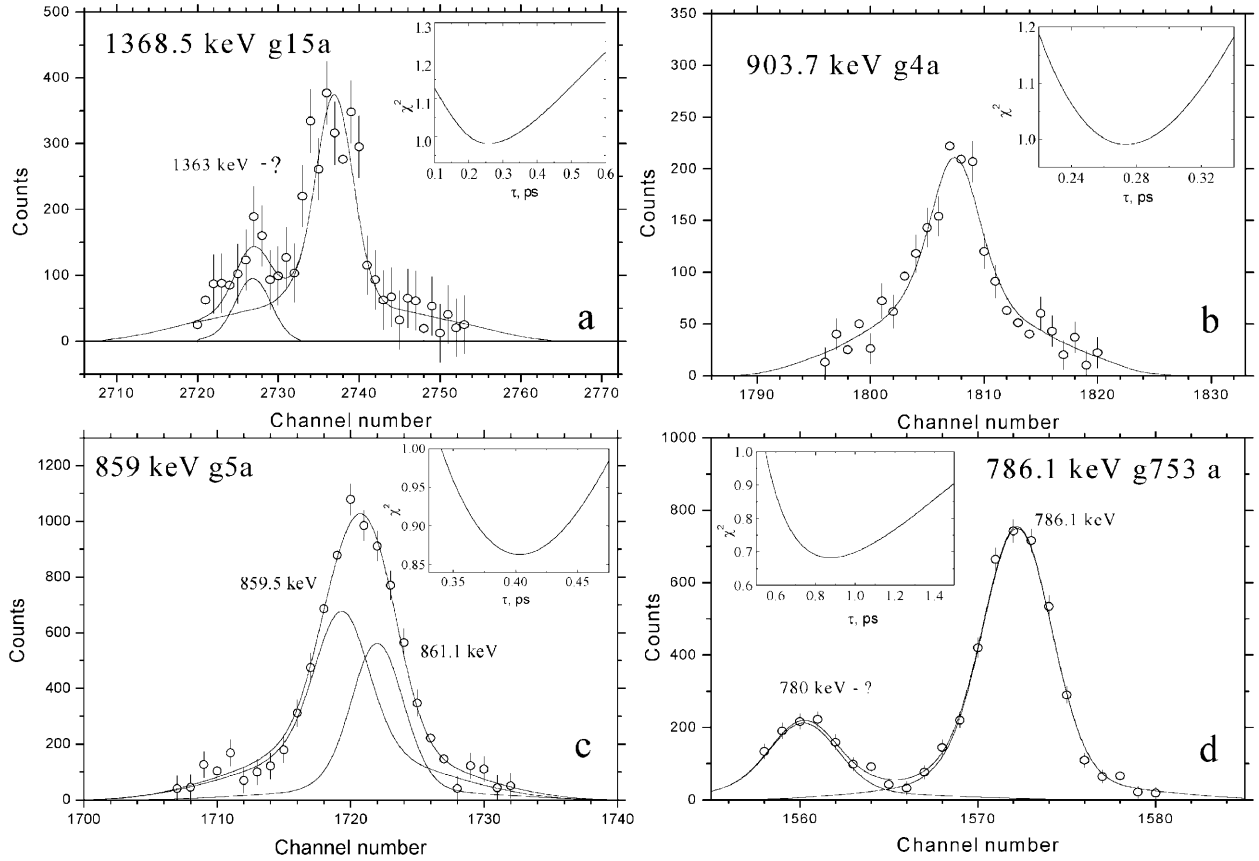

Fig. 5. Results of the DSA analysis for the following states: a) 18^+ (6.715 MeV), b) 14^+ GSB, c) 12^+ GSB and d) 10^+ GSB. See also the description in table 1.

to $1.3^{+0.5}_{-0.4}$ and $0.83^{+0.12}_{-0.08}$ ps, respectively, were given. In ref. [5] the $(\alpha, 2n)$ reaction was used.

4 Discussion

The experimental study of transition probabilities in even-even nuclei using heavy-ion compound nuclear reactions gives mainly the $B(E2)$ values of yrast states. In the $A \approx 120$ mass region yrast levels are usually purely collective up to $I^\pi \approx 10^+$. Above this spin levels belonging to the yrast band have high-spin quasiparticle pair contributions. Above the band crossing the purely collective excitations possess significantly higher energies than the yrast states and may be fragmented over many levels. This makes them practically inaccessible for experimental investigations. In ^{118}Te, in close proximity to the yrast 10^+_1 and 12^+_1 states, there are states with the same spins $(10^+_2, 12^+_2)$ lying above them by 85 and 47 keV, respectively. The small splitting indicates, that the interband interaction is weak. It allows us to identify some levels (see fig. 2) as a continuation of the collective ground-state band above the band crossing [7,5] and gives the unique possibility to analyze the $B(E2)$ values measured in the present work in this energy region.

In outline one can consider the energy spectra of the bands in fig. 2 to be similar to the vibrational pattern though with increasing spin the levels spacing also increases indicating transition to a rotational spectrum. Such spectra are successfully described in the framework of the Interacting Boson Model (IBM) [15]. However IBM cannot be applied here in its "classical" aspect because the description of two-quasiparticle bands is outside its frames. Nevertheless, generalized versions of the model (the Interacting Boson-Fermion Model, IBFM) treating collective and high-spin quasiparticle excitations on an equal footing have been worked out now ([11,16] and references therein) and have resulted in a reasonable description of the interplay of the collective and quasiparticle degrees of freedom in transitional nuclei.

In the present work we follow ref. [11] where: a) the direct and exchange mechanisms in the boson-fermion interaction are taken into account to construct the boson interaction, b) the Quasiparticle Random Phase Approximation (QRPA) is applied to calculate the microscopic two-quasiparticle structure of both collective quadrupole excitations and high-spin ones, fermion counterparts of the IBM d bosons and high-spin bosons, respectively. Then, the calculated two-quasiparticle compositions are used to determine the boson interaction parameters. In the microscopic analysis given in ref. [11] two sets of model parameters were used. One set of IBM parameters describes purely collective states whereas other sets are employed

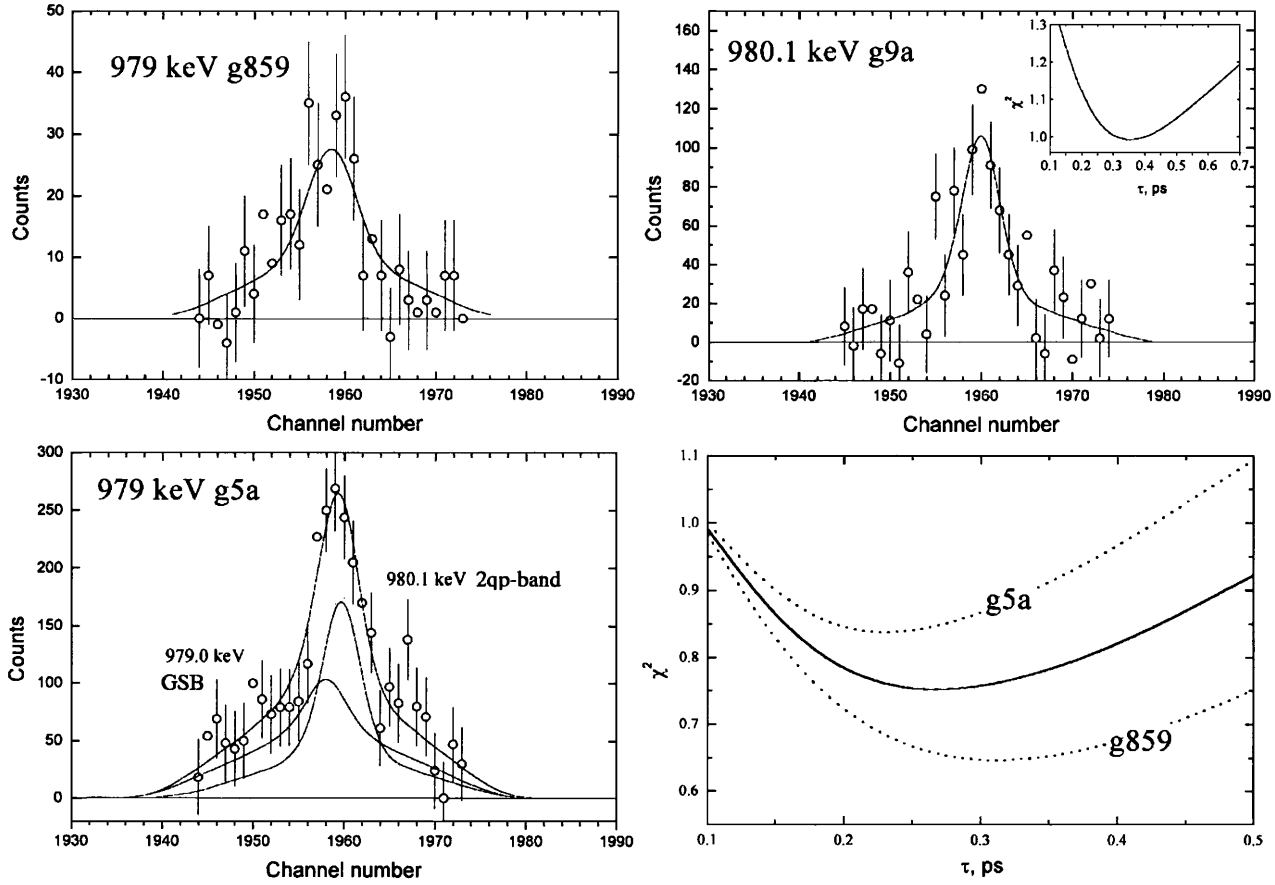

Fig. 6. Results of the DSA analysis of 979.0 keV (16^+ GSB) and 980.1 keV (16^+ 2qp-B) lines. χ^2 panel corresponds to 16^+ GSB. See also caption of fig. 4.

for states with high-spin quasiparticle pair, treated in ref. [11] as high-spin two-quasiparticle excitations. Thus, the blocking of the collective states by an added quasiparticle pair is taken into account phenomenologicaly. This effect depends on the quantum numbers of the nucleons constituting the pair. Nevertheless, for the sake of simplicity in ref. [11] the difference of parameters is considered only for proton and neutron pairs.

Thus, the Hamiltonian describing purely collective boson excitations (s, d) and their interaction with weakly collectivized high-spin bosons (b) reads

$$H = H_0 \left(1 - \sum_{\tau=\mathrm{p,n}} \hat{n}_{\mathrm{b}\tau}\right) + \sum_{\tau=\mathrm{p,n}} H_{(\tau)} \hat{n}_{\mathrm{b}\tau} + H_{\mathrm{b}} + V. \quad (1)$$

The collective IBM Hamiltonians H_0, H_{n}, H_{p} are of the identical form

$$H_{0,\mathrm{n,p}} = \varepsilon_{\mathrm{d}} \hat{n}_{\mathrm{d}} + (k_1 d^+ \cdot d^+ ss + k_2 [d^+ d^+]^{(2)} \cdot ds + \mathrm{H.c.}) + \frac{1}{2} \sum_L C_L [d^+ d^+]^{(L)} \cdot [dd]^{(L)}. \quad (2)$$

They are distinguished by the choice of parameters. In eq. (1) $\hat{n}_{\mathrm{b}\tau}$ denotes the operator of the number of high-spin bosons. Therefore $1 - \sum \hat{n}_{\mathrm{b}\tau}$ and $\hat{n}_{\mathrm{b}\tau}$ provide the projection onto purely collective quadrupole states and states containing a high-spin boson, respectively. H_{b} is a high-spin boson energy and V is an interaction between collective and high-spin bosons. The method for calculating parameters of H_{b} and V was suggested in ref. [11]. The model configuration space comprises Ω s and d bosons in its purely collective part or $\Omega - 1$ s and d bosons in the presence of a high-spin pair. This approach was applied for describing properties of Ba, Ce [11], ^{110}Cd [17] and ^{120}Xe [4] and with some simplifications for a preliminary analysis of ^{118}Te [5].

In the present work calculations are performed with the maximum value of the IBM boson number Ω equal to 9, *i.e.* the half of the valence nucleon number in ^{118}Te. This value will be called hereafter as Ω_{st} (standard). The first set of the IBM parameters (H_0) has been fitted to reproduce almost pure collective states 0_2, 2_1, 2_2, 4_1, 4_2, 6_1 and 8_1. The second set (H_{n}) corresponding to the presence of neutron quasiparticle pairs is determined by the energy levels of the band built on $\nu(h_{11/2})^2$ configuration with spin 10^+. The third set (H_{p}) corresponds to protons. In ^{118}Te there are only two protons outside the closed shell. In the case of high-spin two-quasiproton excitation they cannot take part in collective motion. Therefore, the parameters of H_{p} are determined from properties of ^{116}Sn.

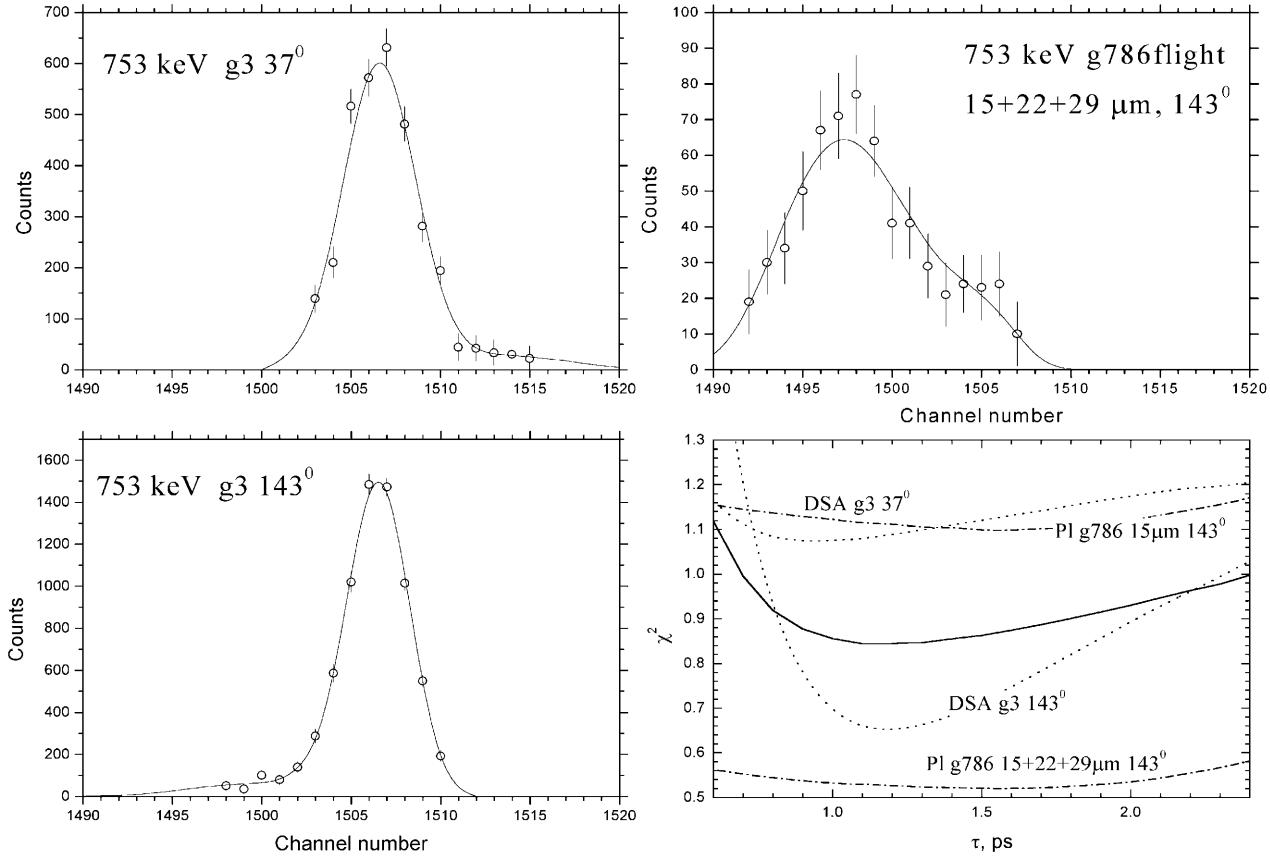

Fig. 7. Lifetime evaluation of the 8^+ level by line shape analysis of DSA (left panels) and plunger spectra. The meaning of χ^2 shown in the bottom right panel is explained in the caption of fig. 4.

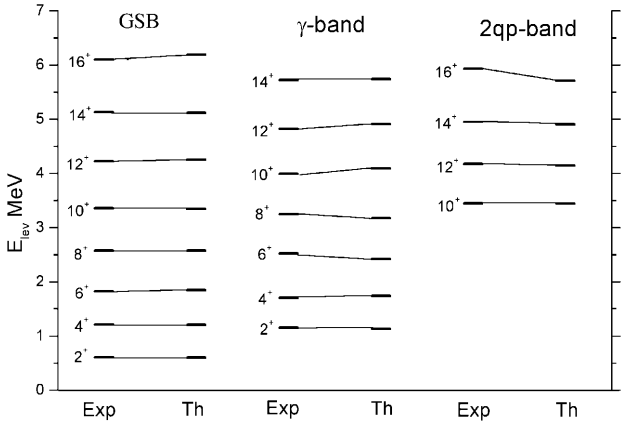

Fig. 8. Comparison of the experimental and theoretical levels schemes (see also table 2).

Owing to the vibrational character of the first collective excitations in this nucleus we address the $SU(5)$ limit of IBM to find the only parameter $\varepsilon_{\rm d}$ (one boson energy) which is fixed from the 2_1^+ energy. The influence of $H_{\rm p}$ on the results is small because of firstly the large transition energies within the two-quasiproton bands and secondly the high excitation energies of the two-quasiproton pairs $(h_{11/2})^2$.

Table 2 and fig. 8 compare the experimental and theoretical energies calculated with the IBM parameters of table 3 and theoretical values of $H_{\rm b}$ and V in eq. (1). The latter is determined with two-quasiparticle amplitudes and energies of table 4. In accordance with ref. [11] each high-spin boson is an image of a two-quasiparticle excitation whose quasiparticle amplitudes for $J^q = 4$ and 6 (J^q is a high-spin boson angular momentum) are presented in table 4. For $J^q \geq 8$ these excitations are mainly $\nu h_{11/2}$ pairs. The collective and high-spin boson composition of the wave functions is given in table 5.

A comparison of the recently published level scheme of ^{118}Te [10] with the results of our calculations allows a new interpretation for many of the levels. In the present work the band GSB in fig. 2 (Band "5" in ref. [10]), is considered as the collective band, where the purely collective component is dominant. However, for the states 14_2^+, 16_3^+ the contributions of other components become comparable. On the top of this band two states with $I^\pi = 18^+$ have been identified experimentally. For one of them, 18_3^+ (7.184 MeV), our calculations predict a significant collective component (see tables 2 and 5). In ref. [10] the ground-state band, up to spin $I = 18^+$, was interpreted as a band with $\beta = 0.17$, $\gamma = -25°$.

Several excited states in ^{118}Te with even I above the 2_2^+ level were observed in ref. [10] and refered to band

Table 2. Energies of excited states (MeV).

Ground-state band			γ-band			2qp-band		
I_i	Exp.	Th.	I_i	Exp.	Th.	I_i	Exp.	Th.
2_1^+	0.606	0.600	2_2^+	1.151	1.131	10_2^+	3.445	3.439
4_1^+	1.206	1.202	4_2^+	1.703	1.735	12_1^+	4.172	4.143
6_1^+	1.821	1.846	6_3^+	2.517	2.418	14_1^+	4.946	4.903
8_1^+	2.574	2.570	8_3^+	3.247	3.171	16_2^+	5.926	5.711
10_1^+	3.360	3.342	10_4^+	3.985	4.085			
12_2^+	4.220	4.250	12_4^+	4.817	4.908			
14_2^+	5.124	5.112	14_4^+	5.721	5.726			
16_3^+	6.103	6.178	16^+	—	6.849			
18_2^+	7.049	7.116						
18_3^+	7.184	7.213						

Table 3. Parameters (in MeV) of collective Hamiltonians; Ω is the boson number.

	$\varepsilon_{\rm d}$	k_1	k_2	C_0	C_2	C_4	Ω
H_0	0.6842	−0.0188	0.012	−0.3469	−0.112	0.0505	9
$H_{\rm n}$	0.7511	−0.005	0.0127	0.3484	−0.1488	0.0326	8
$H_{\rm p}$	1.29	0	0	0	0	0	8

Table 4. Main two-quasiparticle amplitudes A for pair excitations with $J^q = 4$, 6. The energy of pairs $\varepsilon^q(J^q = 4) = 2.144$ MeV and $\varepsilon^q(J^q = 6) = 2.695$ MeV.

Config.	$A(J^q = 4)$	Config.	$A(J^q = 6)$
$\nu(g_{7/2})^2$	−0.22	$\nu(g_{7/2}d_{5/2})$	0.15
$\nu(h_{11/2})^2$	0.55	$\nu(g_{7/2})^2$	0.18
$\nu(s_{1/2}g_{7/2})$	−0.17	$\nu(h_{11/2})^2$	−0.75
$\nu(d_{3/2}d_{5/2})$	0.15	$\pi(g_{7/2}d_{5/2})$	0.40
$\nu(d_{3/2}g_{7/2})$	0.12		
$\pi(d_{5/2})^2$	−0.65		
$\pi(g_{7/2}d_{5/2})$	−0.16		
$\pi(g_{7/2})^2$	0.10		

"Y2" (states 2^+, 4^+) and to band "1" (states 6^+–14^+). We guess, that these states (labeled as "γ-band" in table 2 and fig. 2) can be the members of the γ-band. Firstly, they are characterized in the calculations by large $B(E2)$ values ($\approx$ 50 W.u.) for intraband transitions that is typical for a γ-band in its geometrical interpretation. Secondly, our calculations (table 5) reproducing the energies of these states indicate that their structure on the whole corresponds to the quasi-γ-band in the geometrical model approach, though the states 12_4^+, 14_4^+ in this band reveal a more complicated structure.

We consider the states 10^+ (3.445 MeV), 12^+ (4.172 MeV), 14^+ (4.946 MeV) of band Y2 in ref. [10] and state 16^+ (5.926 MeV) to be members of the same band since the two-quasineutron configuration $\nu[h^2_{11/2}]$ coupled to

Table 5. Wave function amplitudes $A(J^q, L_i)$. The state with total angular momentum I_i (column 1) is classified by J^q — the spin of two-quasiparticle excitation and L_i —the spin of the pure collective d and s boson state. The index "i" is a state ordinal number. The absence of J^q in brackets means the absence of a two-quasiparticle component. The amplitudes with absolute value larger than 0.15 are only presented. The main component of the wave function is marked using bold font. The part of the IBM γ-band with even L is composed mainly of the boson L_2 states.

I_i	Wave function amplitudes $A(J^q, L_i)$			
	Ground-state band			
2_1	**1.00**(2_1)			
4_1	**0.97**(4_1)	0.20(4^q0_1)		
6_1	**0.94**(6_1)	0.31(4^q2_1)		
8_1	**0.90**(8_1)	0.40(4^q4_1)		
10_1	**0.81**(10_1)	−0.23(10_2)	0.48(4^q6_1)	
12_2	**0.80**(12_1)	0.14(12_2)	0.50(4^q8_1)	0.20(10^q2_1)
14_2	**0.65**(14_1)	−0.40(14_2)	0.57(4^q10_1)	−0.16(8^q6_1)
16_3	**0.73**(16_1)	0.58(4^q12_1)	−0.25(8^q8_1)	
18_3	**0.67**(18_1)	0.48(4^q14_1)	0.28(4^q14_3)	−0.28(8^q10_1)
	γ-band			
2_2	**0.99**(2_2)			
4_2	**0.98**(4_2)	0.16(4^q2_1)		
6_3	**0.95**(6_2)	0.18(4^q2_2)		
8_3	−0.18(8_1)	**0.91**(8_2)	0.18(4^q4_1)	0.26(4^q4_2)
10_4	0.39(10_1)	**0.80**(10_2)	−0.21(4^q6_1)	0.24(8^q2_1)
12_4	−0.18(12_1)	**0.65**(12_2)	−0.55(10^q2_2)	0.18(10^q4_1)
14_4	**0.77**(14_3)	0.53(4^q10_2)	0.18(10^q4_2)	
	2qp-band			
10_2	0.13(10_1)	0.13(8^q2_1)	**0.92**(10^q0_1)	−0.31(10^q2_1)
12_1	0.18(8^q4_1)	**0.90**(10^q2_1)	−0.22(10^q2_2)	−0.21 (10^q4_1)
14_1	0.18(8^q6_1)	**0.92**(10^q4_1)	−0.24(10^q4_2)	−0.17 (10^q6_1)
16_2	0.17(8^q8_1)	**0.93**(10^q6_1)	−0.24(10^q6_2)	−0.15 (10^q8_1)

Table 6. Comparison between the experimental and theoretical $B(E2)$ values in ^{118}Te. Values of $B(E2)$ are given in W.u.

$E_{\rm lev}$ (MeV)	E_γ (MeV)	$I_i^\pi \to I_f^\pi$	$B(E2)$ (W.u.)	
			Exp.	Th-2
0.606	0.606	$2_1^+ \to 0_1^+$	33^{+6}_{-5}	35
1.206	0.601	$4_1^+ \to 2_1^+$	69^{+19}_{-11}	64
1.821	0.614	$6_1^+ \to 4_1^+$	80^{+14}_{-10}	86
2.574	0.753	$8_1^+ \to 6_1^+$	82^{+27}_{-20}	102
3.360	0.786	$10_1^+ \to 8_1^+$	91^{+22}_{-20}	111
4.220	0.859	$12_2^+ \to 10_1^+$	127^{+32}_{-21}	108
5.124	0.904	$14_2^+ \to 12_2^+$	141 ± 24	118
6.103	0.979	$16_3^+ \to 14_2^+$	98^{+41}_{-26}	122
5.926	0.980	$16_2^+ \to 14_1^+$	50^{+20}_{-15}	68
5.926	0.802	$16_2^+ \to 14_2^+$	25^{+10}_{-8}	0.1
6.715	1.368	$18_1^+ \to 16_1^+$	18^{+10}_{-6}	—

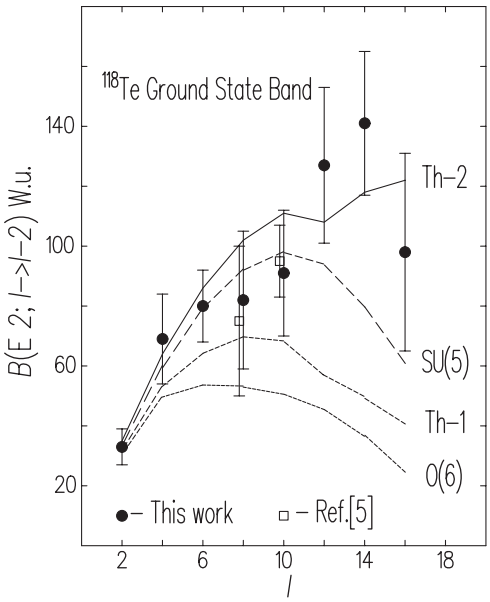

Fig. 9. The comparison of the experimental $B(E2)$ values inside the ground-state band in ^{118}Te with calculations: Th-1 ($\Omega = \Omega_{\rm st} = 9$); Th-2 ($\Omega = \Omega_{\rm st} + 10$), the IBM $SU(5)$ and $O(6)$ limits ($\Omega = \Omega_{\rm st} = 9$).

$I^q = 10^+$ prevails in the wave functions of these states. In tables 2, 5 and figs. 2 and 8 this band is shown as 2qp-band.

An irregularity observed in the level spacing (the low energy of the $16_1^+ \to 14_1^+$ transition; see fig. 2) indicates a loss of collectivity. In ref. [9] the $I^\pi = 16_1^+$ state is assumed to have the fully aligned $\pi[(g_{7/2})^2]_{6+} \otimes \nu[(h_{11/2})^2]_{10+}$ configuration. The band based on this configuration should be similar to the ground-state band in Sn isotopes due to the strong blocking effect of the decoupled protons. The $18_1^+ \to 16_1^+$ transition ($E_\gamma = 1.368$ MeV) has $B(E2; 18_1^+ \to 16_1^+) = 18^{+10}_{-6}$ W.u. (table 6). These values are similar to the $2^+ \to 0^+$ transition in ^{114}Sn, where $E_\gamma = 1.300$ MeV and $B(E2; 2_1^+ \to 0_1^+) = 16^{+4}_{-3}$ W.u. Therefore, the states 16_1 and 18_1 can be considered as the members of a band built on the $\pi[(g_{7/2})^2]_{6+} \otimes \nu[(h_{11/2})^2]_{10+}$ excitation.

Whereas our IBFM calculations of the energy spectrum of ^{118}Te are in agreement with the experiment (table 2, fig. 8) the analysis of the $E2$ probabilities (Th-1 in fig. 9) performed with the eigenfunction of the Hamiltonian, eqs. (1) and (2) and the standard IBM $E2$-transition operator

$$\hat{T}^{(E2)} = e^*(d^+ s + s^+ d + \chi d^+ d)^{(2)} \qquad (3)$$

leads to $B(E2)$ values which evidently disagree with experiment for $I > 10$. The significance of the discrepancy is stressed by the $B(E2)$ calculations in the IBM $SU(5)$ limit with $\Omega = 9$ (fig. 9). At a fixed Ω this limit provides the maximum growth of the $B(E2)$ values *vs.* I as compared with other IBM limits, *e.g.*, $O(6)$, and with any of the intermediate variants. Note that the $SU(5)$ limit is not capable to explain the collective energy spectrum and inband transitions. The curve of Th-1 in fig. 9 is of a typical shape with a maximum predicted by IBM for the yrast $B(E2)$ values. Such an I-dependence of $B(E2)$ can be expressed more explicitly using the unitary equivalent form of the IBM $T^{(E2)}$ operators [18]:

$$\hat{T}^{(E2)} = e^*(d^+\sqrt{\Omega - \hat{n}_{\rm d}} + \sqrt{\Omega - \hat{n}_{\rm d}}\, d + \chi d^+ d)^{(2)} = e'\left(d^+\sqrt{1 - \frac{\hat{n}_{\rm d}}{\Omega}} + \sqrt{1 - \frac{\hat{n}_{\rm d}}{\Omega}}\, d + \chi' d^+ d\right)^{(2)}. \qquad (4)$$

Hence, one straightforwardly obtains, that for transitions between the $SU(5)$ yrast states (in this representation they are $(d^+)^n|0> (\sqrt{n!})^{-1}$, $I = 2n$), $B(E2)$ is maximum at $I \sim \Omega$.

The existence of the maximum boson number Ω is one of the basic ideas of IBM assuming that the collective space is limited by valence shells. Thus, the attenuation of the yrast $B(E2)$'s above $I \simeq \Omega_{\rm st}$ ($\Omega_{\rm st}$ is the half of the valence particle or hole number) could confirm this idea of the finiteness of the collective boson space. In our case such an attenuation is absent. The experimental data indicate an almost monotonous increase. Such an I-dependence of $B(E2)$ is not unique for ^{118}Te. Similar behavior is observed for the two-quasineutron band in ^{120}Xe [4]. Neither of the experimental $B(E2)$ values in ^{126}Ba and ^{130}Ce [11] could be reproduced with $\Omega_{\rm st}$ (eq. (3)).

These examples do not exhaust all types of $B(E2)$ *vs.* I-dependences. There exist nuclei, *e.g.*, ^{74}Se [14], with distinctly pronounced $B(E2)$ attenuation above $I \sim \Omega_{\rm st}$. However, such cases require a special study since one of the reasons for the $B(E2)$ attenuation is the band crossing (that can be revealed on the curves of Th-1 and Th-2 (see text below) in fig. 9 as a shallow local minimum at $I = 12$). Therefore, in nuclei with observed $E2$ attenuation the roles of the band crossing and the finiteness of the boson space have to be explicitly separated.

Table 7. Wave function amplitudes $A(n_{\rm d},\nu)$ of the collective states calculated with H_0 (eq. (2)); $n_{\rm d}$ and ν are the d boson number and seniority (the number of d bosons, which are not pairwise coupled to zero), respectively. I_i is a spin of state with ordinal number i. The absolute values of amplitudes larger than 0.21 are presented.

I_i	$A(n_{\rm d},\nu)$			
0_1	0.89(0,0)	0.43(2,0)		
2_1	0.83(1,1)	0.49(3,1)		
2_2	0.23(1,1)	0.78(2,2)	0.52(4,2)	0.23(6,2)
4_1	0.78(2,2)	0.52(4,2)	0.23(6,2)	
4_2	0.35(2,2)	0.68(3,3)	0.53(5,3)	0.26(7,3)
6_1	0.74(3,3)	−0.23(4,4)	0.54(5,3)	0.25(7,3)
6_2	0.43(3,3)	0.59(4,4)	0.53(6,4)	0.28(8,4)
8_1	0.71(4,4)	−0.26(5,5)	0.56(6,4)	0.25(8,4)
8_2	0.48(4,4)	0.51(5,5)	0.54(7,5)	0.29(9,5)
10_1	0.69(5,5)	−0.28(6,6)	0.58(7,5)	0.25(9,5)
10_2	−0.57(5,5)	−0.22(6,6)	−0.40(8,6)	0.65(9,5)
12_1	0.72(6,6)	−0.29(7,7)	0.60(8,6)	
12_2	0.46(6,6)	0.49(7,7)	−0.23(8,8)	0.71(9,7)
14_1	0.68(7,7)	−0.26(8,8)	0.69(9,7)	
16_1	0.95(8,8)	−0.32(9,9)		
18_1	1.00(9,9)			

Though the experimental data in fig. 9 reveal no attenuation above $I \sim \Omega_{\rm st} = 9$ they could be interpreted in the frame of IBM under some assumptions. Firstly, the form of the IBM $E2$-operator might be extended by adding operators removing its strong Ω-dependence. Such a term was introduced in [11]. Generally, this is the problem of a more precise boson expansion of pair fermion operators. Secondly, the collective space might be wider than the valence shells, which can be caused by residual interactions leading to core polarizations and deformations. Such an idea was discussed for deformed nuclei [19]. The third, more preferable assumption is a gradual or step-wise enlarging of the collective space, *i.e.* Ω, which arises due to mutual influence of low-energy collective excitations and the mean and pairing fields. This occurs in the similar way in the self-consistent cranking model. Thereby the microscopic structure of the collective quadrupole pair (d boson) could alter affecting the IBM parameters and Ω. Such an enlarging of Ω may depend on excitation energy or spin. We have made an attempt to apply the third assumption fitting Ω to reproduce experimental $B(E2)$ values in the whole spin region. This gives a reasonable description of the I-dependence of the $B(E2)$ values, however, it entails an increasing number of the model parameters. Therefore, to remain in the traditional framework of IBM, we assumed that in ^{118}Te the collective space is such that Ω is the same for all states under consideration and larger than $\Omega_{\rm st}$.

Strictly speaking, the larger value of Ω has to be applied in energy and $B(E2)$ calculations. However, in nuclei which are not far from the $SU(5)$ limit of IBM (as ^{118}Te) the increase of Ω does nearly not affect the eigenvalues and eigenfunctions since in the $SU(5)$ limit they are independent of Ω.

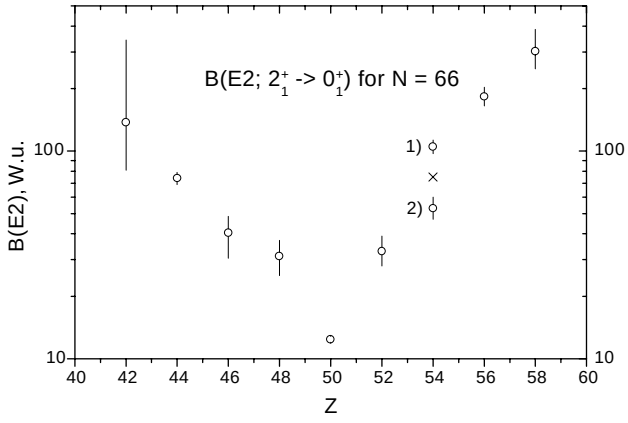

Fig. 10. The values of $B(E2;\, 2_1^+ \to 0_1^+)$ for $N = 66$. 1) and 2) data from refs. [20] and [21], respectively. ×: the result of IBM-1 calculation [4].

In a more general case the same is true if the expectation value of $n_{\rm d}$ does not significantly exceed the value $I/2$. This condition is almost fulfilled for the wave functions calculated with the parameters of table 3. In table 7 the wave functions of the collective states are presented in the $SU(5)$ basis: the yrast states with $I \leq 10$ have at least the main component resulted from states with $n_{\rm d} \sim I/2$, the yrast IBM states with $I > 10$ are practically the $SU(5)$ yrast states and so they are independent of Ω. Besides, the increase of Ω can be compensated by corrections of the model parameters. Our calculations of the energy spectrum with $\Omega > \Omega_{\rm st}$ confirm these arguments. Therefore, we present the energy spectrum calculated with $\Omega = \Omega_{\rm st}$. Since the $B(E2)$ values are more sensitive to the choice of Ω we have tried to find the best value given by $\Omega = \Omega_{\rm st} + 10$. The corresponding curve (Th-2) in fig. 9 indicates much better agreement with experiment than the curve of Th-1 ($\Omega = \Omega_{\rm st}$). The comparison of the experimental and theoretical $B(E2)$ values, corresponding to the Th-2 curve in fig. 9, is given in table 6.

Since in the present work the $B(E2;\, 2_1^+ \to 0_1^+)$ value for ^{118}Te has been measured first time, it is of interest to compare it with available systematics. The experimental $B(E2;\, 2_1^+ \to 0_1^+)$ values for all even isotones with $N = 66$ and $Z = 42$–58 are displayed in fig. 10. We can compare our value with estimates given in ref. [22] where data on $^{112\text{-}128}$Te were analysed to discuss the choice of the effective boson charges. The values of 53 or 44 W.u. predicted in ref. [22] for ^{118}Te are higher than our experimental value (33 ± 5 W.u.).

5 Conclusion

Lifetimes of the ground-state band levels in ^{118}Te with spin values from $I^\pi = 2^+$ up to 16^+ have been measured with the Doppler Shift Attenuation and Recoil Distance methods in the (^{13}C, p3n) reaction at $E = 54$ MeV. A new methodical approach of lifetime extraction, based on precise line shape analysis for both methods has been used.

Experimental level energies and $E2$ probabilities are interpreted in the frame of the IBM1 + 2qp semi-microscopic theory developed in ref. [11]. A comparison of the experimental level scheme with the results of our calculations allows us to find a one-to-one correspondence between theoretical and experimental states. This enables to identify three bands: the ground-state band, two-quasiparticle and quasi-γ bands. The analysis of the $B(E2)$ values forced us to enlarge the maximum boson number beyond the standard IBM value. As a consequence a satisfactory description of the $E2$ probabilities measured in this work is achieved.

We would like to thank A. Gelberg and R.M. Lieder for discussions and critical remarks. Thanks are given to Yu.N. Lobach for a collaboration at an early stage of this work. One of us (AAP) thanks the Mianowski Kasa Foundation and Prof. Z. Zaleski for financial support and hospitality during his stay in Poland. Support from the Danish Natural Science Research Council and the NORDBALL collaboration is acknowledged.

Appendix A. Accuracy of the ^{118}Te RDDSAM analysis for stretched E2 transitions

In case of ^{118}Te the experimental conditions are the same as in the experiment presented in ref. [2], therefore the parameters used in line shape calculation (in particular the recoil's stopping power) and $D_0 = 5.7 \pm 0.3$ μm were taken from that work.

Let us regard in details the lifetimes evaluation of the 6^+, 4^+ and 2^+ states. As an example, in fig. 11 the standard χ^2 plot for 6^+ state is shown, in which as in whole our paper, the χ^2 value is divided by the number of degrees of freedom $N_{\rm DF}$. fig. 11 corresponds to fig. 4 presented at the main part of this paper, but with appropriate enlargement. In the case of the 6^+ level, the 614.3 keV line is not strongly overlapped with the 605.9 keV peak and with two fully shifted contamination lines. Therefore, after preliminary fitting, it was possible to subtract all contamination peaks and to plot total χ^2 curve (see caption of fig. 4) for single 614.3 keV line within 16 channel segment of spectrum. For the total χ^2 plot $N_{\rm DF}$ = number of channels × number of target − stoper distances−number of parameters = 16×4−2 = 62. The lifetime error $\sigma_{\rm S}(6^+)$ was derived, in a standard manner, from the χ^2 level [2] equal to $\chi^2_{\rm min}(1 + 1/N_{\rm DF})$. As a result we evaluated the statistical component of the total error as $\sigma_{\rm S}(6^+) = 0.28$ ps. The component of error, connected with 0.3 μm uncertainty of D_0 is $\sigma_{\rm D} \approx 0.1$ ps for the recoil velocity $v \approx 1\%c$.

To evaluate the influence of cascade feeding on $\tau(6^+)$ the number of calculations have been done under different assumptions of cascade feeding pattern. The calculations show that the main contribution to this error is connected with the uncertainity of the lifetime value of the 8^+ state. Figure 12 presents dependence of the lifetime of the 6^+ state on the lifetime of the 8^+ state. It shows, that the lifetime of the 8^+ level (corresponding to the gating transition) does not strongly affect the value of $\tau(6^+)$ since gating only on shifted component of the 753 keV γ line has been applied. The corresponding part of the error equals $\sigma_{\rm G} \approx 0.13$ ps. Using the formula $\sigma^2_{\rm tot} = \sigma^2_{\rm S} + \sigma^2_{\rm D} + \sigma^2_{\rm G}$ we can roughly estimate the total error $\sigma_{\rm tot}(6^+) \approx 0.3$ ps. It is remarkably less than the value 0.5 ps, given in the table containing final results and in fig. 4. In the case of $\tau(6^+)$ we have increased the final error basing on the "pessimistic" assumption about $\sigma_{\rm S}$ (influence of the background line etc.).

In the case of the 600.6 keV and 605.9 keV overlapping γ lines, which correspond to the decay of the 4^+ and 2^+ states it is impossible to analyse them separately. After subtraction of the small contributions of the 614.3 and 611 keV lines, the χ^2 curves have been plotted taking into account 27 channels. Then, $N_{\rm DF} = 27 \times 6 - 3 = 159$ and $N_{\rm DF} = 27 \times 4 - 3 = 105$ for the 4^+ and 2^+ states, respectively (fig. 4). Each point on the χ^2 curve has been calculated altering the lifetime of the neighbouring peak during the fitting procedure both for the 4^+ and 2^+ states. High sensitivity of χ^2 values to the lifetime parameters is connected with the facts, that during fitting procedure

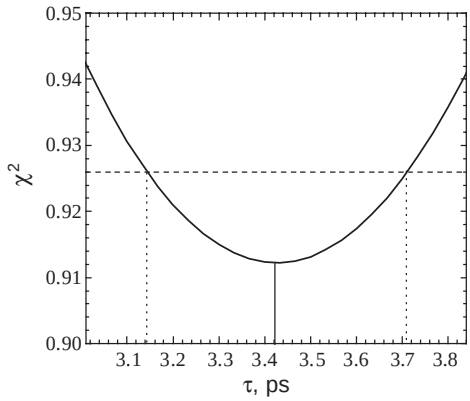

Fig. 11. The plot for the RDDSA lifetime analysis of the 6^+ state in ^{118}Te. The χ^2 value devided by the number of degrees of freedom $N_{\rm DF}$ is presented. The values of $\tau(6^+) = 3.42$ and $\sigma_{\rm S} = 0.28$ ps are deduced.

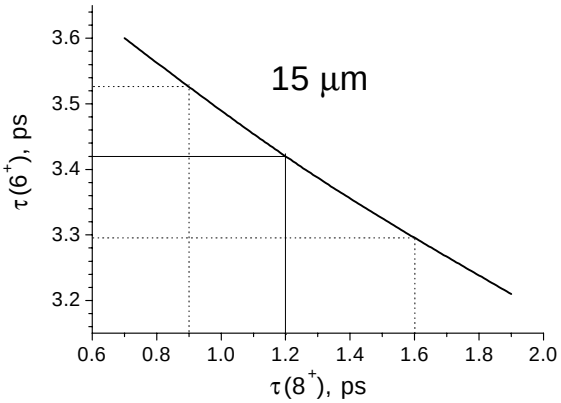

Fig. 12. Dependence of the lifetime of the 6^+ level on the lifetime of the 8^+ level at the distance of 15 μm.

the energies of both peaks were fixed, and the intensities of both overlapping lines have been assumed to be equal (due to gating above the level of interest).

The influence of uncertainty of the 8^+ state lifetime on the 4^+ and 2^+ state lifetimes, has been determined. For both cases the $\sigma_{\rm G}$ values do not exceed ≈ 0.1 ps. This is due to following correlation —the increase (decrease) of $\tau(8^+)$ leads to decrease (increase) of $\tau(6^+)$. This effect compensates partly the influence of $\tau(8^+)$ and $\tau(6^+)$ on the lifetime of levels lying in cascade below the 8^+ and 6^+ states. Main sources of additional errors for considered cases are the statistical errors of lifetimes of the upper transitions. For the 4^+ state it is the statistical error $\sigma_{\tau 6}(4^+)$ connected with the uncertainty of $\tau(6^+)$ state.

For the 2^+ state there are both statistical errors $\sigma_{\tau 6}(2^+)$ and $\sigma_{\tau 4}(2^+)$ connected with unceraintly of $\tau(6^+)$ and $\tau(4^+)$. Assuming the "optimistic" variants for error evaluation we have $\sigma^2_{\rm tot}(4^+) = \sigma^2_{\rm S}(4^+) + \sigma^2_{\rm D} + \sigma^2_{\rm G} + \sigma^2_{\tau 6}(4^+)$ and $\sigma^2_{\rm tot}(2^+) = \sigma^2_{\rm S}(2^+) + \sigma^2_{\rm D} + \sigma^2_{\rm G} + \sigma^2_{\tau 6}(2^+) + \sigma^2_{\tau 4}(2^+)$. Therefore, $\sigma_{\rm tot}(4^+) \approx 0.6$ ps and $\sigma_{\rm tot}(2^+) \approx 1.1$ ps for $\sigma_{\rm S}(4^+) = 0.54$ ps and $\sigma_{\rm S}(2^+) = 0.90$ ps . The errors given in the table 1 are larger then these shown above due to pessimistic assumption about $\sigma_{\rm S}$. As it was shown, in the case of spectra gated above, RDDSAM only sligtly depends on cascade pattern and when D_0 is precisely measured can give more accurate results than DDCM [23,24].

Appendix B. Notes on the differential decay curve and recoil distance Doppler shift attenuation methods

Here we discuss the Differential Decay Curve Method (DDCM) [23,24] often used nowadays, and the method used in the present paper —the Recoil Distance Doppler Shift Attenuation Method (RDDSAM). In the "classical" Recoil Distance Method the lifetime extraction is based on decay curve analysis

$$R(D_i) = I_{\rm u}(D_i)/(I_{\rm u}(D_i) + I_{\rm s}(D_i))\,,$$

where D_i is the distance between target and stopper, $I_{\rm u}(D)$ and $I_{\rm s}(D)$ are intensities (at distance D_i) of unshifted and shifted components of a γ line of interest, respectively. The Differential Decay Curve Method can be considered (from the point of view of its simplicity) as variant of the "classical" method since only intensities of shifted and unshifted components are needed. In the DDCM method for each distance D_i the value of $\tau(D_i) = I_{\rm u}(D_i)/(v \times I'_{\rm s}(D_i))$ has to be extracted, where v is the recoil velocity and $I'_{\rm s}(D)$ is the derivative of the $I_{\rm s}(D)$-dependence. The final result τ is the mean value of $\tau(D_i)$. The DDCM has important advantage: independence from the systematical shift of measured target-stopper distance D_0.

Limitations of the DDCM are following: satisfactory separation between shifted and unshifted components and easiness of background subtraction are indispensable to get reliable information on $I_{\rm u}$ and $I'_{\rm s}$. This requirement imposes limitation on target thickness, recoil velocity, energy of γ-transition and detector resolution.

From the point of view of the statistical accuracy the error of the evaluated time $\tau(D_i)$ in DDCM is larger even in comparison to the value, extracted from $R(D_i)$ due to the presence of derivative $I'_{\rm s}(D)$ in the DDCM formula instead of the absolute value and larger than in the case of RDDSAM (the line shape analysis). In the case of the above-mentioned suitable conditions the statistical errors specific to DDCM can be small.

The advantages of the RDDSAM are the following: i) no need to separate γ lines for shifted and unshifted components, because both components are analysed simultanously treating lifetimes as line shape parameters, ii) possibility to analyze lines with relatively small Doppler shift. There are no strong requirements on target thickness, recoil velocity, energy of γ-transition and detector resolution, iii) for small τ this analysis becomes automatically the DSAM one, iv) high accuracy and reliability of results can be achieved due to possibility of χ^2 analysis at each distance D_i, v) for RDDSAM in comparison to DDCM there is no need to measure spectra at many distances D_i in sensitive region since there is no need to use derivative $I'_{\rm s}$. Limitations of the RDDSAM are the following: i) all factors which influence the line shape (*e.g.*, stopping power) should be well known, ii) D_0 should be known.

In both discussed methods the cascade feeding as well as side feeding are the serious problems in the case when analysed spectra are gated below the transition of interest. As it was shown in our paper (and it is the same for DDCM) it is not the case when gate is put on the shifted component of the transition placed above transition of interest. Other "profit" from the spectra obtained in such manner is that intensity of stretched $E2$ transitions located below the gate are equal. This is important for getting of reliable results in the case of overlapping Doppler-broadened peaks.

References

1. Yu.N. Lobach, A.A. Pasternak, J. Srebrny, Ch. Droste, G.B. Hagemann, S. Juutinen, T. Morek, M. Piiparinen, E.O. Podsvirova, S. Törmänen, K. Starosta, A. Virtanen, A. Wasilewski, Acta Phys. Pol. B **30**, 1273 (1999).
2. J. Srebrny, Ch. Droste, T. Morek, K. Starosta, A. Wasilewski, A.A. Pasternak, E.O. Podsvirova, Yu.N. Lobach, G.B. Hagemann, S. Juutinen, M. Piiparinen, S. Törmänen, A. Virtanen Nucl. Phys. A **683**, 21 (2001).
3. A.A. Pasternak, E.O. Podsvirova, J. Srebrny, Ch. Droste, T. Morek, K. Starosta, G.B. Hagemann, S. Juutinen, M. Piiparinen, S. Törmänen, A. Virtanen, Yu.N. Lobach, Acta Phys. Pol. B **31**, 439 (2000).
4. A.A. Pasternak, Y. Sasaki, A.D. Efimov, V.M. Mikhajlov, T. Hayakawa, Y. Toh, M. Oshima, Y. Hatsukawa, J. Katakura, N. Shinohara, Z. Liu, K. Furuno, Eur. Phys. J. A **9**, 293 (2000).
5. A.D. Efimov, Yu.N. Lobach, Yad. Fiz. V **61**, 3 (1998).

6. P.C. Chowdhury, W.F. Piel Jr, D.B. Fossan, Phys. Rev. C **25**, 813 (1982).
7. Van J.J. Ruyvan, W.H.A. Hesselink, J. Akkermans, Van P. Nes, H. Verheul, Nucl. Phys. A **380**, 125 (1982).
8. A. Sharma, J. Singh, H. Kaur, J. Goswamy, D. Mehta, N. Singh, R.K. Bhowmik, P.N. Trehan, Z. Phys. A **351**, 131 (1995).
9. A. Sharma, J. Singh, H. Kaur, J. Goswamy, D. Mehta, N. Singh, P.N. Trehan, E.S. Paul, R.K. Bhowmik, Z. Phys. A **354**, 147 (1996).
10. S. Juutinen, A. Savelius, P.T. Greenlees, K. Helariutta, P. Julin, P. Jämsen, H. Kankaanpää, M. Muikku, M. Piiparinen, S. Törmänen, M. Matsuzaki, Phys. Rev. C **61**, 014312 (2000).
11. A.D. Efimov, V.M. Mikhajlov, Phys. Rev. C **59**, 3153 (1999).
12. I.Kh. Lemberg, A.A. Pasternak, in *Modern Methods of Nuclear Spectroscopy* (Nauka, 1985) p. 3.
13. G.M. Gusinsky, I.Kh. Lemberg, A.S. Mishin, A.A. Pasternak, in *Modern Methods of Nuclear Spectroscopy* (Nauka, 1985) p. 64.
14. J. Adam, M. Honusek, A. Spalek, D.N. Dojnikov, A.D. Efimov, M.F. Kudojarov, I.Kh. Lemberg, A.A. Pasternak, O.K. Vorov, U.Y. Zhovliev, Z. Phys. A **332**, 143 (1989).
15. F. Iachello, P.Van Isaker, *The Interacting Boson-Fermion Model* (Cambridge University Press, Cambridge, 1991).
16. D. Vretenar, S. Brant, G. Bonsignori, L. Corradini, C.M. Petrache, Phys. Rev. C **57**, 675 (1998).
17. Yu.N. Lobach, A.D. Efimov, A.A. Pasternak, Eur. Phys. J. A **6**, 131 (1999).
18. D. Janssen, R.V. Jolos, F. Dönau, Nucl. Phys. A **224**, 93 (1974).
19. R.F. Casten, A. Aprahamian, Phys. Rev. C **29**, 1919 (1984).
20. J.C. Walpe, B.F. Davis, S. Naguleswaran, W. Reviol, U. Garg, Xing-Wang Pan, Da Hsuan Feng, J.X. Saladin, Phys. Rev. C **52**, 1792 (1995).
21. W. Kutschera, W. Dehnhardt, O.C. Kistner, P. Kump, B. Povh, H.J. Sann, Phys. Rev. C **5**, 1658 (1972).
22. J. Rikovska, N.J. Stone, P.M. Walker, W.B. Walters, Nucl. Phys. A **505**, 145 (1989).
23. A. Dewald, S. Harissoupulos, P. von Brentano, Z. Phys. A **334**, 163 (1989).
24. O. Stuch, K. Jessen, R.S Chakrawarty, A. Dewald, R. Kühn, R. Krucken, P. Petkov, R. Peusequens, H. Tiesler, D. Weil, I. Widenhöver, K.O. Zell, P. von Brentano, C. Ender, T. Hartlein, F. Köck, O. Koschorek, P. Reiter, Phys. Rev. C **61**, 044325 (2001).